

Acoustic Power Absorption and its Relation with Vector Magnetic Field of a Sunspot

S. Gosain · S. K. Mathew ·
P. Venkatakrishnan

© Springer

Abstract The distribution of acoustic power over sunspots shows an enhanced absorption near the umbra–penumbra boundary. Earlier studies revealed that the region of enhanced absorption coincides with the region of strongest transverse potential field. The aim of this paper is to *i*) utilize the high-resolution vector magnetograms derived using *Hinode* SOT/SP observations and study the relationship between the vector magnetic field and power absorption and *ii*) study the variation of power absorption in sunspot penumbrae due to the presence of spine-like radial structures. It is found that *i*) both potential and observed transverse fields peak at a similar radial distance from the center of the sunspot, and *ii*) the magnitude of the transverse field, derived from *Hinode* observations, is much larger than the potential transverse field derived from SOHO/MDI longitudinal field observations. In the penumbra, the radial structures called spines (intra-spines) have stronger (weaker) field strength and are more vertical (horizontal). The absorption of acoustic power in the spine and intra-spine shows different behaviour with the absorption being larger in the spine as compared to the intra-spine.

Keywords: sunspots; magnetic field; *p*-mode absorption; acoustic waves; field inclination

1. Introduction

In the recent years, helioseismic observations of the Sun, meant to study the solar interior, have been used extensively to study the *p*-mode interaction with surface magnetic fields. It is known that the *p*-mode amplitude is suppressed in sunspots and in regions of strong magnetic field (Leighton, Noyes, and Simon, 1962; Lites, White, and Packman, 1982). This reduction in *p*-mode amplitude is attributed to the absorption of acoustic waves by the magnetic structures (Cally, 1995). In fact, observations show that the amplitude of *p*-mode oscillations decreases while the amplitude of high-frequency oscillations increases with increasing line-of-sight (LOS) magnetic field, with a transition near the acoustic-cutoff of 5.3 mHz

Udaipur Solar Observatory, Post Box 198, Dewali,
Udaipur-313001, India email: sgosain@prl.res.in

(Hindman and Brown, 1998; Venkatakrishnan, Kumar, and Tripathy, 2002). Further, the incoming acoustic power was seen to be greater than outgoing power, which implies absorption of acoustic energy by magnetic structures. About 50% of the energy of acoustic p -modes is absorbed in the regions of magnetic-field concentrations like sunspots (Braun, Duvall, and Labonte, 1987; Braun, Duvall, and Labonte, 1988).

The acoustic-power absorption in sunspots could be a valuable tool for probing the sub-photospheric structure of the sunspot magnetic field, once the physical processes responsible for the absorption are understood. Two theories have been proposed to explain this absorption. The first proposal is that of resonant absorption based on strong dissipation of MHD waves in a sunspot flux tube resulting in a net loss of energy. The resonant absorption has been well studied in coronal loops (Ionson, 1982; Hollweg, 1984; Davila, 1987). The second proposal is that of mode conversion, where the incoming acoustic energy is transferred through mode conversion into magnetic wave-modes (Hindman, Jain, and Zweibel, 1997). These waves can leak from the system, either upwards through chromosphere (De Pontieu, Erdélyi, and James, 2004), or downward through the base of the sunspot. However, both of these processes (*i.e.*, the resonant absorption and mode conversion) do not exclude each other and may be operating simultaneously.

The acoustic-power distribution in sunspots shows an enhanced absorption of power near the umbra–penumbra boundary (Mathew, 2008). Further, this region of enhanced absorption was shown to coincide with the region where the mean inclination is about 45 degrees and the transverse field is maximum (Mathew, 2008). The inclination angle and transverse fields were however obtained by computing the potential field using line-of-sight field from SOHO/MDI. With the availability of high-quality vector magnetic-field observations by *Hinode*/SOT, we can now study the relationship between the vector magnetic field and the distribution of acoustic power in a sunspot.

In this paper, we study the relationship between the vector magnetic field and the acoustic-power absorption in different structures of a sunspot. The radial, as well as the azimuthal, variation of magnetic parameters and power absorption is studied. Also, we compare the observed and potential transverse field of a sunspot. Section 2 describes the observational data, its reduction, and analysis. Section 3 describes the results and in the last section we discuss the results and present conclusions.

2. Observations

In order to compare the vector magnetic-field parameters of a sunspot and the acoustic signals, we selected an observational data set which satisfies the following criteria: *i*) The observations must be simultaneous, *ii*) a simple circular unipolar sunspot should be selected as the azimuthal symmetry simplifies our analysis, and *iii*) the sunspot should be located close to disk center for minimal projection effects.

2.1. SOHO/MDI observations

The data for a sunspot in NOAA AR 10960 at the disk center ($\mu=0.98$) on 08 June 2007 08:59 – 10:58 UT met our criteria. These dopplergrams were obtained by SOHO/MDI using high-resolution mode with an image scale of 0.6 arc-sec per pixel. Solar rotation was removed by alignment of images using image cross-correlation technique. The slowly varying component of the velocity signal was removed by doing a running difference *i.e.*, subtracting consecutive dopplergrams. Thus, a time series of two hours with one-minute cadence, which corresponds to a frequency resolution of 0.13 mHz, was constructed. The resulting power spectra at three locations in the umbra, penumbra and the surrounding moat region is shown in Figure 1. The peak corresponding to the dominant five minute oscillations can be noticed clearly and this peak is seen to decrease with increasing field strength in the umbra. Also, we note that the spectrum is quite noisy (left panels). To improve the signal-to-noise ratio we reduce the spectral resolution.

For each pixel we split a single N point time series $T_1 = [1, 2, 3, \dots, N]$ into k smaller time series of size n such that $t_1 = [1, 2, 3, \dots, n]$, $t_2 = [2, 3, \dots, n+1]$, $t_k = [N-n, \dots, N]$ and add power spectra for each of the k time series. This power spectra is then divided by the number N to obtain an average power spectra. Although this operation reduces the frequency resolution (0.52 mHz in our case for $N=118$, $n=33$ and $k=80$), the power spectra becomes less noisy. The peak of the power spectrum is well defined for the smoothed spectra as compared to the multiple peaks in the raw power spectra. The power maps are constructed by summing the power in the band 1.6 to 6.6 mHz. The choice of n is made such that we have sufficient number of sample points in the spectral band 1.6 to 6.6 mHz for making power map. We arrive at $n=33$ which leads to about 10 data points in the spectral band. Choosing n too small would not lead to smooth power spectra while choosing n too large would not lead to sufficient number of data points in spectral band 1.6 to 6.6 mHz.

2.2. Hinode SOT/SP observations

The space-based *Hinode*/SOT observes active regions with the onboard Spectropolarimeter (SP) in the Fe I 630.15 nm and 630.25 nm line pair (Kosugi *et al.*, 2007; Lites *et al.*, 2007; Tsuneta *et al.*, 2008; Ichimoto *et al.*, 2008). A map of an active region is made by scanning the slit of the spectrograph. First, the Stokes profiles were inverted using the “HeLiX” inversion code (Lagg *et al.*, 2004) to generate magnetic maps of the scanned region. This inversion code fits the observed Stokes profiles with synthetic ones that are obtained from an analytic solution of the Unno-Rachkovsky equations under Milne-Eddington model atmosphere assumptions (Unno, 1956; Rachkovsky, 1972; Landolfi and Landi Degl’Innocenti, 1982). The model atmosphere used in our present inversion included a single component atmosphere with a stray-light component. Further, the azimuthal ambiguity of transverse-field component was resolved using the acute angle method (Harvey, 1969). The magnetic-field vectors were then transformed from observed to the local solar reference frame using the procedure

described by Venkatakrishnan and Gary (1989). The region corresponding to the sunspot was extracted from the MDI continuum images and the intensity map from *Hinode*/SP was re-scaled and registered to match the MDI image. Before registration, the spatial resolution of *Hinode*/SP continuum images was degraded to the MDI resolution. The fine registration was done by cross-correlating the two images. The radial and azimuthal variations of the observed parameters of the two registered datasets are studied and the results are presented.

3. Results

3.1. Azimuthal Average of Parameters and their Radial Variation

The radial variation of the observed parameters is shown in Figure 2. The concentric rings, spaced 1.2 arcsec apart, shown in the top panel, represent the paths along which the various parameters are averaged. These mean values are then plotted in the lower panels with increasing radial distance from the center of the rings. The standard deviation (1σ) of these fluctuations is represented by the length of the vertical bars plotted over the mean radial profiles. The mean profiles for continuum intensity, line-of-sight field, field strength and field inclination show a smooth variation with radial distance. However, the acoustic-power in the 1.6 to 6.6 mHz band shows a discontinuous behaviour at the umbra–penumbra boundary. As one approaches umbra–penumbra boundary there is a region of little enhancement followed by region of reduction in acoustic power. This effect was also seen earlier in the study of a different sunspot (Mathew, 2008).

Further, the solid curve in the bottom right panel in Figure 2 shows the variation of observed transverse field with radial distance. The potential transverse field, calculated using the MDI line-of-sight (LOS) field as boundary conditions, is shown with dot-dashed curve. The potential transverse field is significantly underestimated as compared to the transverse field observed by SOT/SP due to different measurement techniques as well as different spatial and spectral resolutions of the two instruments. The cross comparison of the magnetic field measurements by the SOHO/MDI and SOT/SP instruments shows that the field strength in MDI observations is underestimated by about 70% (Wang *et al.*, 2009). An underestimate of the potential transverse field derived from MDI observations as compared to transverse field derived from the *Hinode* SOT/SP observations, shown in the right panel of the bottom row in Figure 2, approximately follows a similar relation. It may be noted that the MDI magnetogram observations that are used in the present work are level 1.8.1 magnetograms which have been corrected for spatially dependent sensitivity variations as determined by Tran *et al.* (2005), leading to an increase in flux values by a factor of about 1.7, as compared to level 1.8.0 magnetograms. More recent (level 1.8.2) magnetograms have been further corrected for sensitivity variations, determined by Ulrich *et al.* (2009). According to these new calibrations the flux values at the disk center reduce by about 8% and limb values reduce by about 30 %. The sunspot in the present study is located close to disk center ($\mu=0.98$). So, the flux values in the (level 1.8.1) magnetograms used in this study may change

by about 8%. Further, we note that in a parallel study Demidov and Baltsar (2009) has suggested that the re-calibration of MDI magnetograms is perhaps not straightforward and that more detailed studies are required. Irrespective of the magnitude of the MDI field, we can see that both curves in the bottom right panel in Figure 2 show the location of enhanced p -mode power absorption and maximum transverse field occur at a similar radial distance from the sunspot umbra. This distance is marked by the vertical dashed line in all panels of Figure 2. The inclination of the magnetic field at this location is also about 135 degrees (or -45 degrees). This is in agreement with the previous results (Mathew, 2008).

From the profiles of magnetic parameters and acoustic power, shown in Figure 2, it can be seen that on the right-hand-side (RHS) of the vertical dashed line the magnetic parameters, as well as the acoustic power, follows a smooth variation such that any of the magnetic parameters can be correlated or anti-correlated with the the acoustic power. While the profile on the left-hand-side (LHS) of the vertical dashed line exhibits no clear relation between the magnetic parameters and acoustic power. This implies that none of the magnetic parameters can fully explain the acoustic power absorption in the entire sunspot. However, to compare the relative importance of the magnetic parameters for acoustic power absorption in a sunspot, we do a correlation analysis of these parameters in the following section.

3.2. Magnetic Parameters versus Acoustic Power Absorption in Different Regions of Sunspot

Here we study the relation between different magnetic parameters and acoustic power absorption in the entire sunspot as well as in different regions of the sunspot. We isolate three regions in a sunspot, *i.e.*, umbra, umbra-penumbra boundary and penumbra, using continuum intensity thresholds. These regions are shown by the contours in Figure 3. The scatterplot of the magnetic-field strength, transverse field, and inclination angle *versus* acoustic power absorption is shown in Figure 4 for these regions. The top panel shows the scatterplot for the entire sunspot area *i.e.*, pixels within the outermost contour. Second, third, and fourth panel from the top, in Figure 4, show the scatterplot for the umbra, umbra-penumbra boundary and penumbra, respectively.

We compute the linear Pearson correlation coefficient (R) between the acoustic power and the magnetic parameters for different regions of the sunspot using the relation

$$R = \frac{\frac{1}{N} \sum_{i=1}^N (P_i - \bar{P})(M_i - \bar{M})}{\sigma_P \sigma_M} \times 100$$

Where, the numerator gives the covariance between the acoustic power P and one of the magnetic parameters M (*i.e.*, field strength, transverse field strength or inclination angle). While, the denominator is the product of the standard deviation of P and M , given by σ_P and σ_M respectively. This correlation coefficient shows the goodness of fit for a linear model (*i.e.*, a measure of the dispersion of data points from a linear slope). For the whole sunspot, we find that there is an anti-correlation between the acoustic power and all of the three parameters *i.e.*, the

field strength (65%), the transverse field (61%) and the field inclination (34%). While in the umbra the scatter is rather flat showing weaker anti-correlation of 6%, 12%, and 10% between acoustic power and field strength, transverse field and field inclination, respectively. For the umbra–penumbra boundary, which corresponds to the region of enhanced absorption of p -mode power, the acoustic power is smaller as compared to the umbra and here also the anti-correlation is weaker *i.e.*, 16%, 17% and 15% between acoustic power and field strength, transverse field and field inclination, respectively. While in the penumbra, the acoustic power is anti-correlated with field strength, transverse field, and field inclination by 46%, 50%, and 13%, respectively.

Thus, the maximum anti-correlation of acoustic power is with the field strength in the entire sunspot, while it is with the transverse field in the penumbral region. The correlation of acoustic power with the field inclination remains weak in general.

3.3. Azimuthal Variation of Parameters along mid-Penumbra

Figure 5 shows maps of various observed parameters of the sunspot: the continuum image, transverse field, field strength, acoustic-power, and field inclination. Figure 6 shows the azimuthal variation of various parameters along the ring marked by the white circle in Figure 5. The location of this ring corresponds to the mid-penumbra, with radius of ~ 8.5 arcsec. In figure 6 the variation of acoustic power and the magnetic parameters show an anti-correlation. Further, the relation between the field strength and inclination suggests that the stronger fields are more vertical as compared to the weaker fields, which are more horizontal. A similar relation was found by Schunker *et al.* (2005). This anti-correlation of B and γ leads to stronger modulation in the LOS field component $B\cos\gamma$. This modulation is seen in MDI-LOS magnetograms and SOT/SP inclination maps as radial spine-like structures in penumbra, previously identified by Lites *et al.* (1993).

A spine structure and its adjacent channel (intra-spine) are marked by two radial line segments in the middle and bottom panels of Figure 5. These two locations are marked in the azimuthal profiles plotted in Figure 6 by vertical lines. The spine (intra-spine) is characterized by stronger (weaker) and vertical (horizontal) fields. The acoustic power absorption in the spine structure is clearly larger than in the intra-spine. The spine corresponds to a field strength of 1400 Gauss and inclination of 145° while the intra-spine corresponds to a field strength of 1100 Gauss and inclination of 112° .

3.4. Radial Variation of the Parameters along Spine and Intra-spine

In view of the azimuthal variations in magnetic and acoustic parameters due to radial spine-like structures, discussed in Section 3.3 above, we make a comparison of the radial variation of these parameters along the spine and intra-spine structure. To this end, we plot the profiles of magnetic parameters and acoustic power along two radial line segments shown in middle and bottom panels of Figure 5. The two line segments correspond to spine and intra-spine, going clockwise along

the white circle. The variation of the parameters along these magnetic structures is shown in Figure 7. The solid (dashed) line curve corresponds to the intra-spine (spine). It may be noted that as compared to the mean radial profiles shown in Figure 2, the radial extent in Figure 7 is limited to 9.6 arcsec. The reason is that, this radial spine and intra-spine extend as coherent structures upto 9.6 arcsec and beyond this distance other structures from the outer penumbra start to show up, while we are interested in the run of parameters along the spine and intra spine.

The parameters differ in the spine and intra-spine, specially beyond the vertical dashed line which marks the umbra–penumbra boundary. Further, it may be noticed that, as compared to the spine, the field strength is weaker in the intra-spine while the transverse field is stronger. However, we see that the power is much reduced in the spine as compared to the intra-spine. This result suggests that the power absorption in magnetic structures is not simply related to the transverse component of the magnetic field, as previously suggested (Mathew, 2008). This is also apparent from the behaviour of the mean profiles of the transverse field and acoustic-power absorption, shown in the bottom panels of Figure 2. That is, while the profile of the transverse field on the right, and left-hand-side of the vertical dashed line is symmetric, the profile of the acoustic-power is not.

4. Discussion and Conclusions

We have used simultaneous MDI and *Hinode* SOT/SP observations of a sunspot, near the disk center, to study the relationship between the magnetic-field vector and the p -mode absorption. Comparing the values of the potential transverse field derived from MDI-LOS field and the transverse field derived from SOT/SP observations, it is found that the former are significantly lower than the latter. This is attributed to different sensitivities (spatial and spectral) of the two instruments as well as different inversion methods. Further, the observed decrease is consistent with the decrease found by the study of the two magnetograms by Wang *et al.* (2009).

The azimuthally averaged radial profiles of field strength and inclination show a smoothly decreasing profile, going outwards from the umbra, in the sunspot. However, the acoustic power absorption does not show such a smooth behaviour. At the umbra–penumbra boundary there is a ring of enhanced p -mode power absorption, in agreement with the earlier study (Mathew, 2008). In that study it was shown, using the potential transverse field, that this region of enhanced absorption is the region of strongest transverse field with mean field inclination of about 45 degrees. However, the availability of SOT/SP vector magnetograms allowed us to carry out a similar study with observed transverse field. It was found that: *i*) the maximum of potential transverse field and observed transverse field peak at a similar radial distance in the sunspot, *ii*) this location coincides with the region where the acoustic power is reduced, and *iii*) the profile of the acoustic power and transverse field are not similar as one goes from the location of the peak transverse field towards the umbra.

The azimuthal profile over the mid-penumbra, *i.e.* along a ring of radius 8.5 arcsec, shows that there is significant variation in power absorption and magnetic

parameters in a sunspot penumbra. We examine two adjacent channels one with stronger field strength (1400 G) and more vertical field (about 145 degrees) than the other channel with slightly weaker field strength (1100 G) and more horizontal fields (about 112 degrees). Such inhomogeneous channels show up clearly as radial spines and intra-spines in MDI LOS maps and are much sharper in SOT/SP inclination maps. The power absorption is greater in the channel with larger field strength, *i.e.* the spine.

The presence of azimuthal inhomogeneity prompted us to look for the radial variation of magnetic and acoustic parameters in these channels, *i.e.* in the spine and intra-spine. The field is stronger (weaker) and vertical (horizontal) in the spine (intra-spine). However, the transverse-field component is stronger in the intra-spine as compared to the spine. The acoustic-power absorption is larger in the spine, *i.e.* the channel with weaker transverse field. These results suggest that the transverse field alone may not govern the acoustic power absorption in the magnetic structures, as suggested by Mathew (2008) from the coincidence of maximum transverse field and enhanced p -mode power absorption in the mean radial profiles of a sunspot.

In a sunspot, the magnetic-field strength and field inclination have a strong anti-correlation (Schunker *et al.*, 2005). So, it is difficult to say if the difference in absorption of acoustic signal in spines and intra-spines is due to different field strengths or different field inclinations or combination of both. From our study of the correlation between the acoustic power and magnetic parameters in different regions of the sunspot, it was found that for the entire sunspot the anti-correlation between acoustic power and field strength is highest (65%), while it is lowest with the inclination (35%).

Further, very high-resolution observations have shown that apart from the spine and intra-spine structure of the penumbra, the penumbral filaments possess structure in the form of dark cores (widths ≈ 90 km) accompanied by lateral brightening (Scharmer *et al.*, 2002). Further, the radial variation of the field inclination is quite different in the dark cores as compared to the lateral bright component of the penumbral filaments (Langhans *et al.*, 2005). It would be interesting to study the acoustic-power absorption by the small-scale features like these dark cores in the penumbral filaments using the time series of high-resolution dopplergrams, in future.

The leakage of p -modes into the upper atmosphere has been widely studied. Waves with periods around five minutes were reported near the footpoints of coronal loops (Berghmans and Clette, 1999; De Moortel *et al.*, 2002). It was suggested that these waves could be associated with p -modes (De Pontieu, Erdélyi, and De Moortel, 2005). The formation of spicules is now believed to be due to leakage of p -modes which is found to be more favourable when field lines are inclined (De Pontieu, Erdélyi, and James, 2004). For a given level of p -mode excitation, the power of acoustic waves will decrease with increase in the leakage of the p -modes. Why then do the intra-spines which are more inclined field (112 degrees) show more acoustic power than the spines which are less inclined (145 degrees)? A simple-minded explanation might be given as follows. The suppression of convection by magnetic fields in a highly conducting plasma is well known, and also it is known that convection in rolls is possible wherever

the magnetic field has large inclination to the gravity vector (Chandrasekhar, 1961; Parker, 1979). Thus, the increase in power of five minute oscillations with inclination could be due to convective motions, which presumably excite the oscillations, and are more vigorous in regions of large field inclination.

Another wave phenomenon seen in chromospheric images of sunspots is that of running penumbral waves (RPW) discovered by Zirin and Stein (1972). These are seen as bright circular fronts originating at the umbra–penumbra boundary and moving towards outer edge of penumbra with an interval of 300 seconds. Recent studies suggest these waves to be slow-mode waves propagating along the field lines (Bloomfield, Lagg, and Solanki, 2007). Further, it is suggested that the chromospheric oscillations with five minute periods at umbra–penumbra boundary may arise because of the field inclination becoming favourable for p -mode power to tunnel through acoustic cut-off (De Pontieu, Erdélyi, and James, 2004). The co-existence of the observed reduction in p -mode power and the excitation of RPWs at the umbra–penumbra boundary suggests the possibility of a connection between these two effects. Application of wavelet analysis can bring out the episodal relationship between a time-dependent variation of the modal power and the excitation of the RPWs. This investigation will be deferred to a future paper.

Further, to rule out instrumental effects we plan to extend the present study using more observations from different instruments like (i) using the intensity-grams from Solar Optical Telescope (SOT) onboard *Hinode* mission (Kosugi *et al.* 2007) and (ii) dopplergrams from Helioseismic and Magnetic Imager (HMI) onboard Solar Dynamics Observatory (SDO) (Scherrer and HMI Team 2002).

Acknowledgements We thank the anonymous referee for their valuable comments and suggestions, which helped to improve the quality of the paper. Also, the authors thank the SOHO/MDI consortia for their data. SOHO is a joint project by ESA and NASA. *Hinode* is a Japanese mission developed and launched by ISAS/JAXA, with NAOJ as domestic partner and NASA and STFC (UK) as international partners. It is operated by these agencies in co-operation with ESA and NSC (Norway).

References

- Berghmans, D. and Clette, F.: 1999, *Solar Phys.* **186**, 207.
 Braun, D.C., Duvall, T.L., Jr., and Labonte, B.J.: 1987, *Astrophys. J.* **319**, L27.
 Braun, D.C., Duvall, T.L., Jr., and Labonte, B.J.: 1988, *Astrophys. J.* **335**, 1015.
 Bloomfield, D.S., Lagg, A., and Solanki, S.K.: 2007, *Astrophys. J.* **671**, 1005.
 Cally, P.S.: 1995, *Astrophys. J.* **451**, 372.
 Chandrasekhar, S.: 1961, “*Hydromagnetic and hydrodynamic instability*”, International Series of Monographs on Physics, Oxford University Press, 1961.
 Davila, J.M.: 1987, *Astrophys. J.* **317**, 514.
 De Moortel, I., Ireland, J., Hood, A.W., and Walsh, R.W.: 2002, *Astron. Astroph.* **387**, L13.
 De Pontieu, B., Erdélyi, R., and James, S.P.: 2004, *Nature* **430**, 536.
 De Pontieu, B., Erdélyi, R., and De Moortel, I.: 2005, *Astrophys. J.* **624**, L61.
 Demidov, M.L. and Balthasar, H.: 2009, *Solar Phys.* **260**, 261.
 Harvey, J.W.: 1969, *Ph.D. Thesis*.
 Hindman, B.W. and Brown, T.M.: 1998, *Astrophys. J.* **504**, 1029.
 Hindman, B.W., Jain, R., and Zweibel, E.G.: 1997, *Astrophys. J.* **476**, 392.
 Hollweg, J.V.: 1984, *Astrophys. J.* **277**, 392.

- Ichimoto, K., Lites, B., Elmore, D., Suematsu, Y., Tsuneta, S., Katsukawa, Y., Shimizu, T., Shine, R., Tarbell, T., Title, A., Kiyohara, J., Shinoda, K., Card, G., Lecinski, A., Streander, K., Nakagiri, M., Miyashita, M., Noguchi, M., Hoffmann, C., and Cruz, T.: 2008, *Solar Phys.* **249**, 233.
- Ionson, J.A.: 1982, *Astrophys. J.* **254**, 318.
- Kosugi, T., Matsuzaki, K., Sakao, T., Shimizu, T., Sone, Y., Tachikawa, S., Hashimoto, T., Minesugi, K., Ohnishi, A., Yamada, T., Tsuneta, S., Hara, H., Ichimoto, K., Suematsu, Y., Shimojo, M., Watanabe, T., Shimada, S., Davis, J.M., Hill, L.D., Owens, J.K., Title, A.M., Culhane, J.L., Harra, L.K., Doschek, G.A., and Golub, L.: 2007, *Solar Phys.* **243**, 3.
- Lagg, A., Woch, J., Krupp, N., and Solanki, S.K.: 2004, *Astron. Astroph.* **414**, 1109.
- Landolfi, M. and Landi Degl’Innocenti, E.: 1982, *Solar Phys.* **78**, 355.
- Langhans, K., Scharmer, G.B., Kiselman, D., Löfdahl, M.G., and Berger, T.E.: 2005, *Astron. Astroph.* **436**, 1087.
- Leighton, R.B., Noyes, R.W., and Simon, G.W.: 1962, *Astrophys. J.* **135**, 474.
- Lites, B.W., White, O.R., and Packman, D.: 1982, *Astrophys. J.* **253**, 386.
- Lites, B.W., Elmore, D.F., Seagraves, P., and Skumanich, A.P.: 1993, *Astrophys. J.* **418**, 928.
- Lites, B.W., Elmore, D.F., Streander, K.V., Hoffmann, C.M., Tarbell, T.D., Title, A.M., Shine, R.A., Ichimoto, K., Tsuneta, S., Shimizu, T., and Suematsu, Y.: 2007, In: Shibata, K., Nagata, S., and Sakurai, T. (eds.) *New Solar Physics with Solar-B Mission* **369**, 55.
- Mathew, S.K.: 2008, *Solar Phys.* **251**, 515.
- Parker, E.N.: 1979, *“Cosmical Magnetic Fields”*, Oxford University Press, 1979.
- Rachkovsky, D.N.: 1972, *Izvestiya Ordena Trudovogo Krasnogo Znameni Krymskoj Astrofizicheskoy Observatorii* **44**, 64.
- Scharmer, G.B., Gudiksen, B.V., Kiselman, D., Löfdahl, M.G., and Rouppe van der Voort, L.H.M.: 2002, *Nature* **420**, 151.
- Scherrer, P. H., & SDO/HMI Team. 2002, in Bulletin of the American Astronomical Society, Vol. 34, Bulletin of the American Astronomical Society, 735.
- Schunker, H., Braun, D.C., Cally, P.S., and Lindsey, C.: 2005, *Astrophys. J.* **621**, L149.
- Tran, T., Bertello, L., Ulrich, R.K., and Evans, S.: 2005, *The Astrophysical Journal Supplement Series* **156**, 295.
- Tsuneta, S., Ichimoto, K., Katsukawa, Y., Nagata, S., Otsubo, M., Shimizu, T., Suematsu, Y., Nakagiri, M., Noguchi, M., Tarbell, T., Title, A., Shine, R., Rosenberg, W., Hoffmann, C., Jurcevich, B., Kushner, G., Levay, M., Lites, B., Elmore, D., Matsushita, T., Kawaguchi, N., Saito, H., Mikami, I., Hill, L.D., and Owens, J.K.: 2008, *Solar Phys.* **249**, 167.
- Ulrich, R.K., Bertello, L., Boyden, J.E., and Webster, L.: 2009, *Solar Phys.* **255**, 53.
- Unno, W.: 1956, *Publications of the Astronomical Society of Japan* **8**, 108.
- Venkatakrishnan, P. and Gary, G.A.: 1989, *Solar Phys.* **120**, 235.
- Venkatakrishnan, P., Kumar, B., and Tripathy, S.C.: 2001, *Solar Phys.* **202**, 229.
- Venkatakrishnan, P., Kumar, B., and Tripathy, S.C.: 2002, *Solar Phys.* **211**, 77.
- Wang, D., Zhang, M., Li, H., and Zhang, H.Q.: 2009, *Solar Phys.* **260**, 233.
- Zirin, H. and Stein, A.: 1972, *Astrophys. J.* **178**, L85.

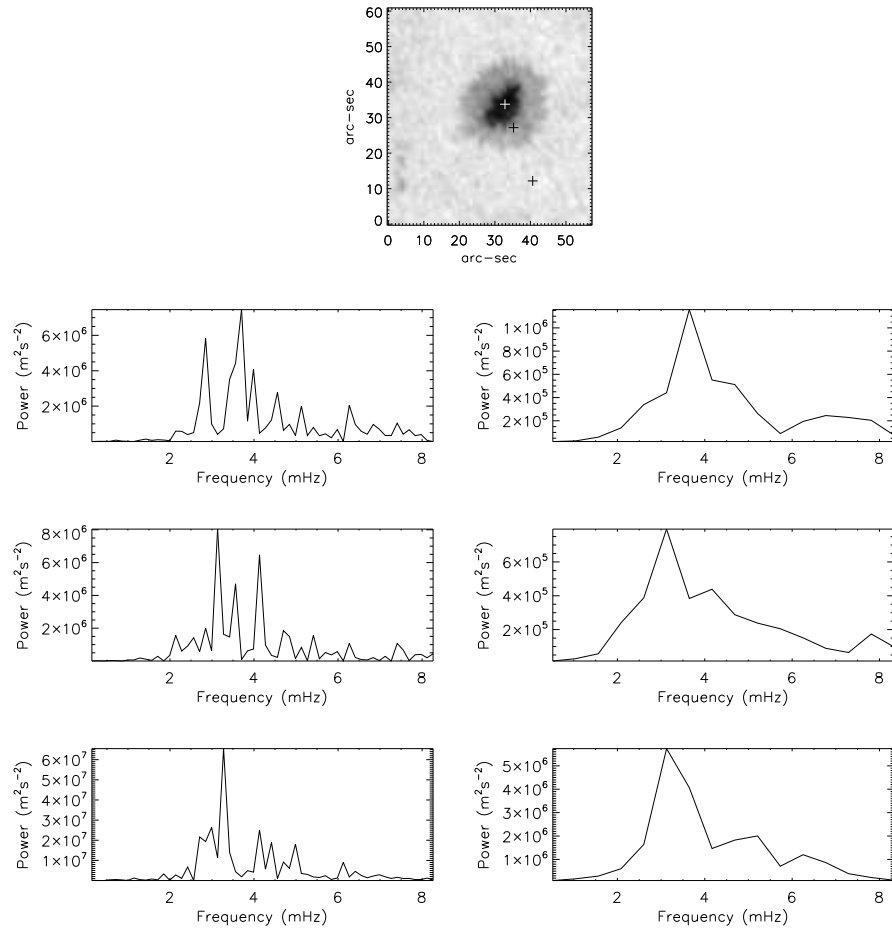


Figure 1. The continuum MDI image of the sunspot with three points marked in umbra, penumbra, and outside the sunspot is shown at the top. The power spectra without (left) and with smoothing (right) for the three points marked on the image above. The top, middle and bottom row correspond to umbra, penumbra, and point outside the sunspot.

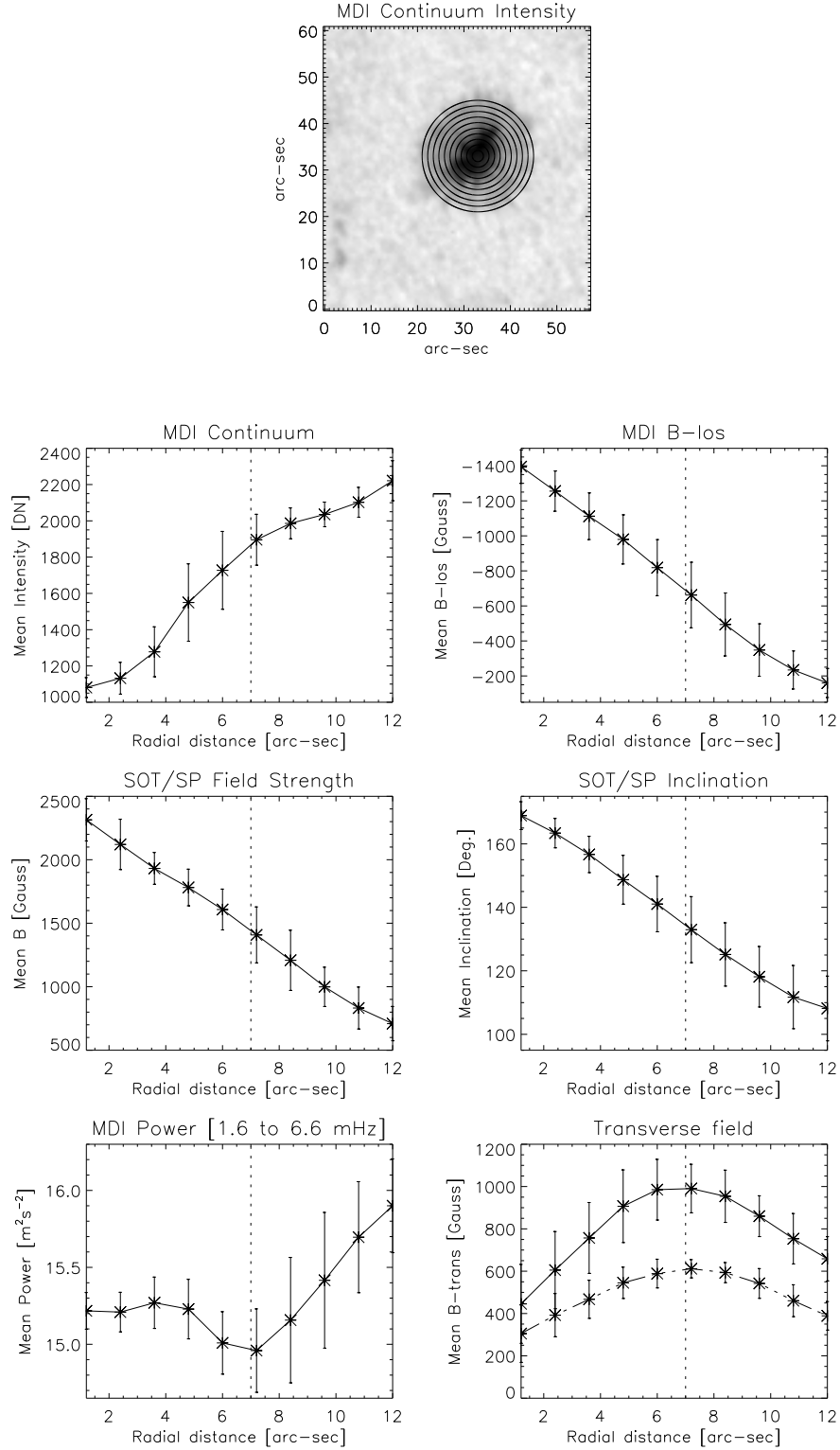


Figure 2. Concentric rings with increasing radius drawn over sunspot as shown in the upper panel are used for studying the radial variation of different parameters. The average value of the parameters is calculated along each ring which is plotted in the lower panels. The radial distance from the center of the sunspot is given in arcsec. The right panel in the bottom row represents observed transverse field (*solid line*) and potential transverse field computed using line-of-sight field measured by MDI (*dash-dotted line*). The vertical dashed line in all panels marks the location of enhanced power absorption.

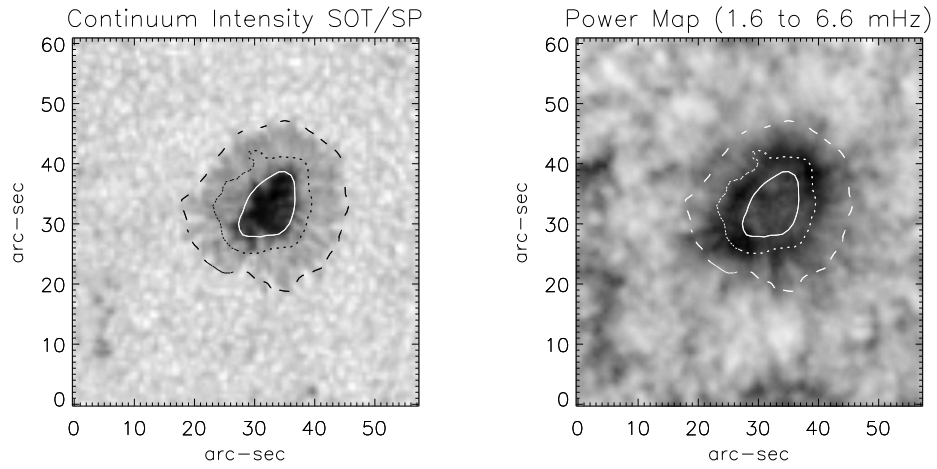


Figure 3. The continuum intensity levels used to isolate the three regions *i.e.*, umbra, umbra-penumbra boundary, and penumbra. These region bounds are shown by solid, dotted and dashed contours over the SOT/SP continuum-intensity image (left) and acoustic-power map (right), respectively.

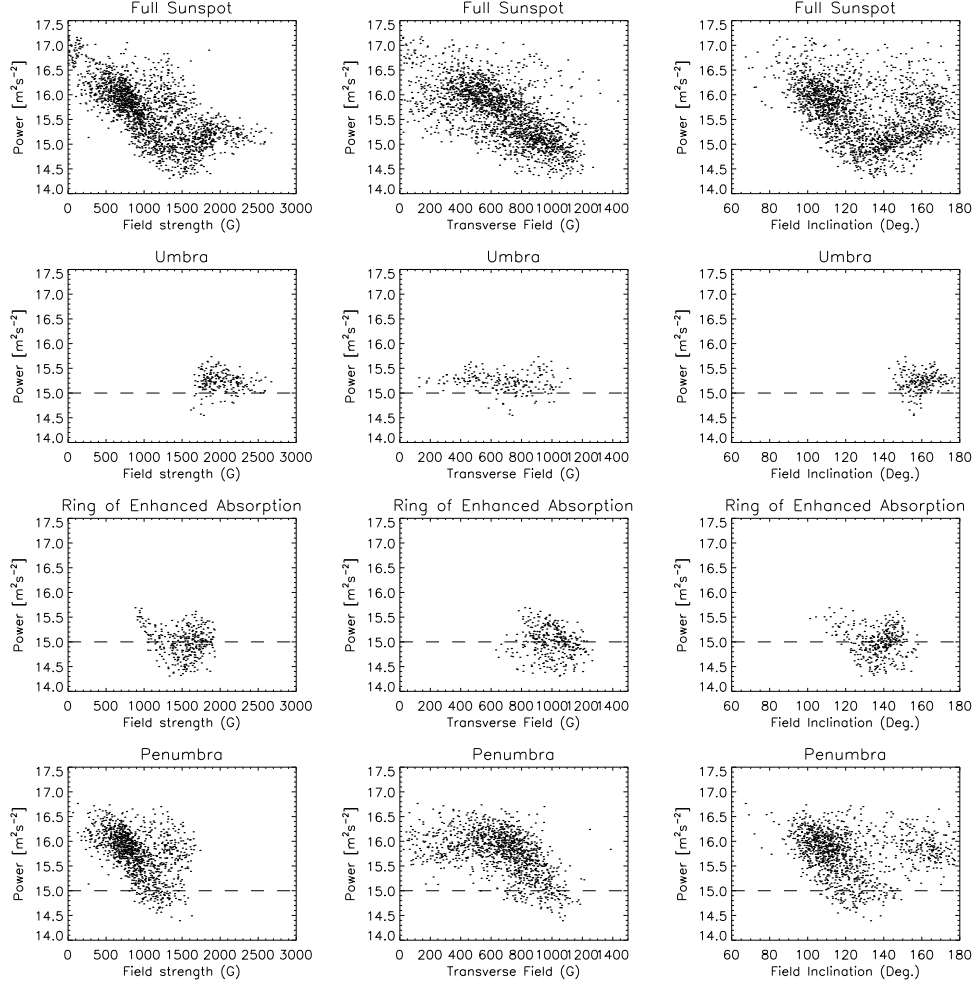


Figure 4. The scatter between acoustic-power absorption and field strength, transverse field, and inclination angle. The scatterplots for the full sunspot, umbra, umbra-penumbra boundary, and penumbra are shown from top to bottom.

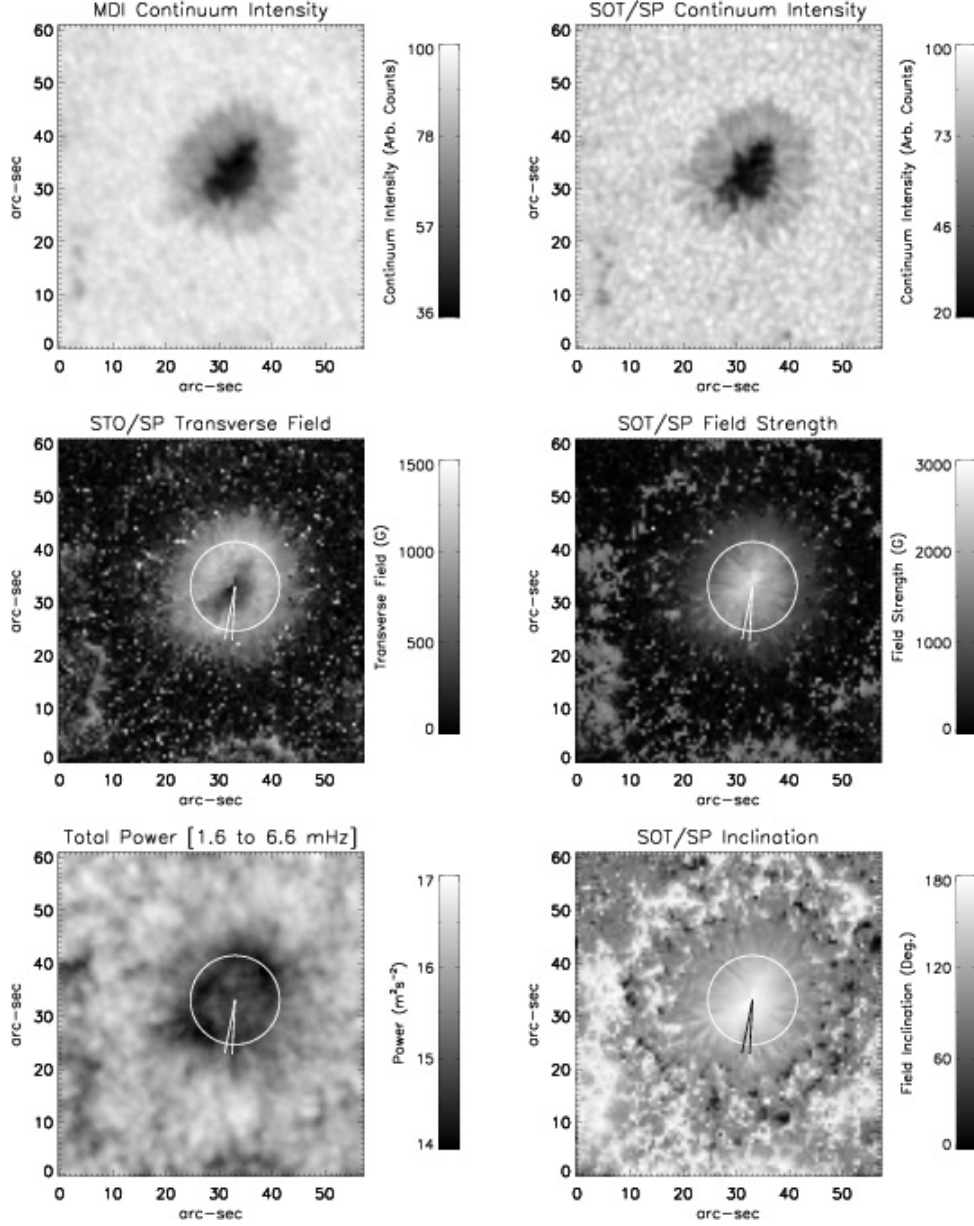


Figure 5. *Top row:* Continuum intensity image of the sunspot by MDI (left panel) and SOT/SP (right panel). *Middle row:* transverse field (left) and field strength (right) maps obtained by SOT/SP observations. *Bottom row:* the MDI acoustic power map (left) and magnetic field inclination (right). The white circle marks the location for which the azimuthal profile is plotted in Figure 6. The two radial line segments in the middle and bottom rows mark the azimuth positions of a spine and intra-spine (going clockwise along white circle). These positions are drawn as vertical lines in Figure 4. The profile of the parameters along these two line segments is shown in Figure 7.

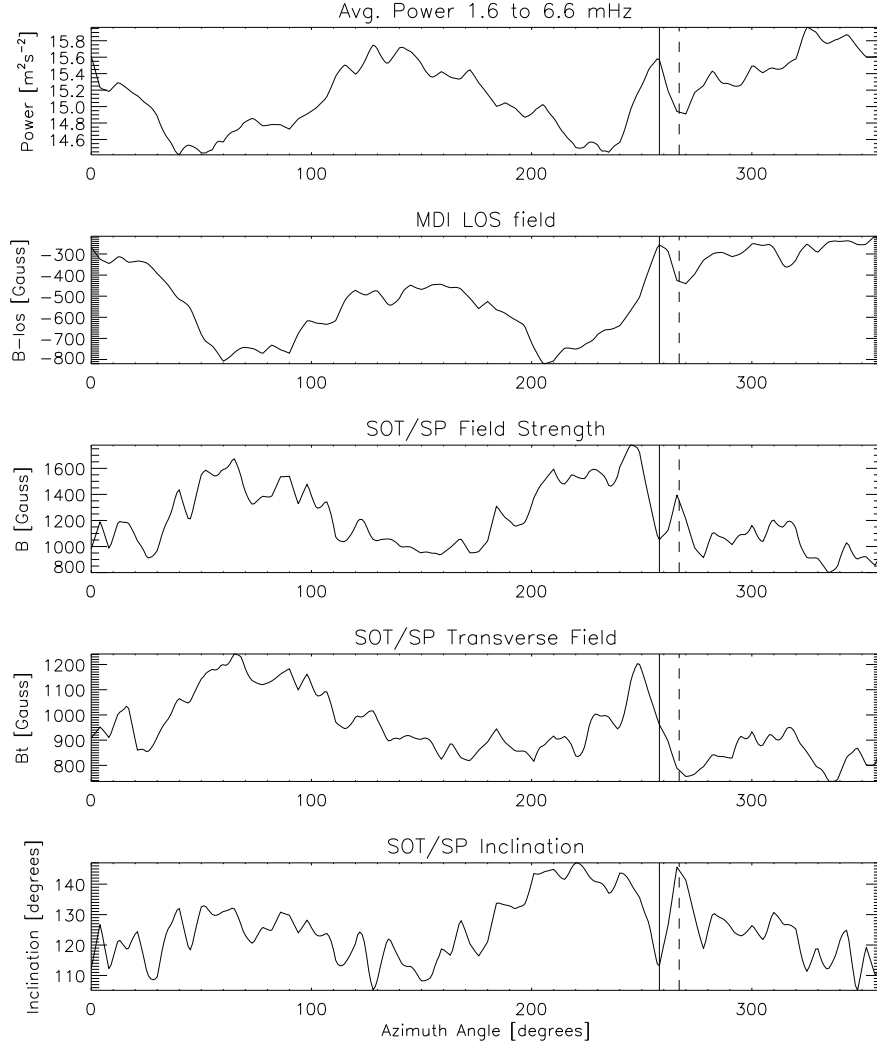


Figure 6. The azimuthal variation of the parameters along the white circle of radius 8.5 arcsec in the lower panels of Figure 3. The vertical lines, one solid and one dashed, correspond to intra-spine and spine structures in the penumbra, respectively. The panels from top to bottom represent maps of *i*) mean acoustic power in the band 1.6 to 6.6 mHz, *ii*) MDI B-los, *iii*) SOT/SP field strength, *iv*) SOT/SP transverse field strength and *v*) the SOT/SP field inclination.

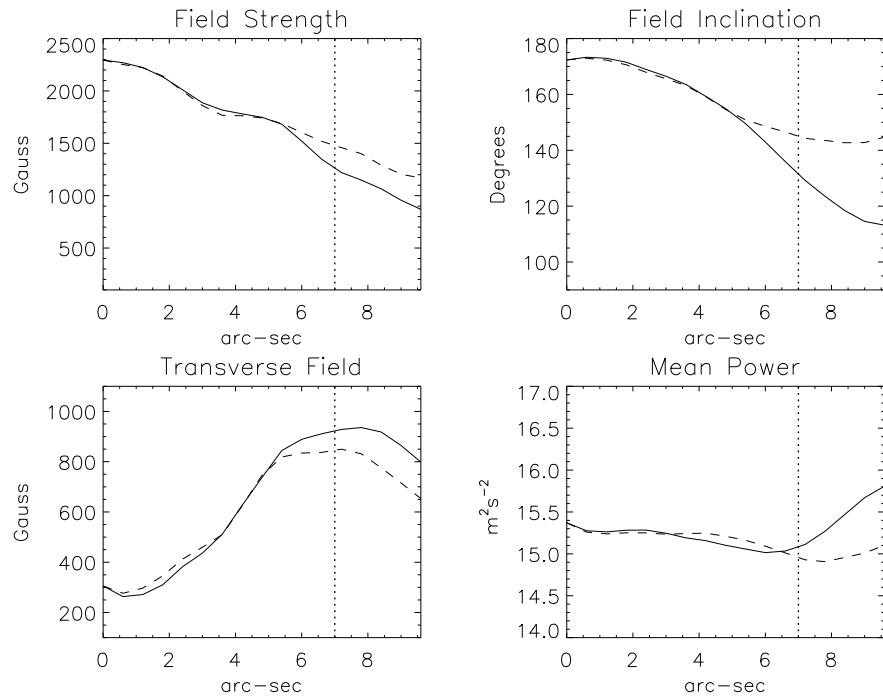


Figure 7. The radial profiles of the parameters along the two radial line segments in the bottom panels of Figure 3. The solid (dashed) line corresponds to intra-spine (spine). The vertical dashed line corresponds to the location of enhanced power absorption in the mean azimuthal profile of Figure 2.

